RESEARCH ARTICLE

NANO · MICRO small
www.small-journal.com

Swarms of Enzyme-Powered Nanomotors Enhance the Diffusion of Macromolecules in Viscous Media

*Noelia Ruiz-González, David Esporrín-Ubieto, Ana C. Hortelao, Juan C. Fraire, Anna C. Bakenecker, Marta Guri-Canals, Ramón Cugat, José María Carrillo, Montserrat Garcia-Batlletbó, Patricia Laiz, Tania Patiño, and Samuel Sánchez**

Over the past decades, the development of nanoparticles (NPs) to increase the efficiency of clinical treatments has been subject of intense research. Yet, most NPs have been reported to possess low efficacy as their actuation is hindered by biological barriers. For instance, synovial fluid (SF) present in the joints is mainly composed of hyaluronic acid (HA). These viscous media pose a challenge for many applications in nanomedicine, as passive NPs tend to become trapped in complex networks, which reduces their ability to reach the target location. This problem can be addressed by using active NPs (nanomotors, NMs) that are self-propelled by enzymatic reactions, although the development of enzyme-powered NMs, capable of navigating these viscous environments, remains a considerable challenge. Here, the synergistic effects of two NMs troops, namely hyaluronidase NMs (HyaNMs, Troop 1) and urease NMs (UrNMs, Troop 2) are demonstrated. Troop 1 interacts with the SF by reducing its viscosity, thus allowing Troop 2 to swim more easily through the SF. Through their collective motion, Troop 2 increases the diffusion of macromolecules. These results pave the way for more widespread use of enzyme-powered NMs, e.g., for treating joint injuries and improving therapeutic effectiveness compared with traditional methods.

1. Introduction

The development of drug delivery systems with high therapeutic efficacy and reduced side effects has been a long-standing challenge in biomedicine.[1] Particularly, passive nanoparticles (NPs) have been explored to act as drug carriers. Yet, they still need to overcome complex scenarios, such as viscous media,[2–4] the extracellular matrix (ECM), mucus, or synovial fluid (SF) in the joints, to name a few. These structures are highly complex and are mainly composed of hyaluronic acid (HA), glycoproteins, and collagen, with a high viscosity that reduces the ability of conventional nonmotile carriers to reach their target site. Hence, there is a clear need for novel, disruptive, and more efficient nanomedicine technologies capable of increasing the penetration and diffusion efficiency facing biological environments. In this context, self-propelled NPs, namely nanomotors (NMs), hold great potential to overcome the low diffusion problem. However, NMs have mostly been studied in liquids such as water, phosphate buffer solution (PBS), or Newtonian fluids, while their actuation in complex biofluids remains poorly explored. In this context, most studies based on micro- and nanomotors capable of swimming in high-viscosity media rely upon externally driven forces, such as magnetic control. Accordingly, examples showing diverse materials can be found in the literature,

N. Ruiz-González, D. Esporrín-Ubieto, A. C. Hortelao, J. C. Fraire, A. C. Bakenecker, M. Guri-Canals, S. Sánchez
Institute for Bioengineering of Catalonia (IBEC)
Barcelona Institute of Science and Technology (BIST)
Baldiri i Reixac 10-12, Barcelona 08028, Spain
E-mail: nruiz@ibecbarcelona.eu; ssanchez@ibecbarcelona.eu

R. Cugat
Mutualidad de Futbolistas – Delegación Catalana
Federación Española de Fútbol
Barcelona 08010, Spain

The ORCID identification number(s) for the author(s) of this article can be found under https://doi.org/10.1002/smll.202309387

DOI: 10.1002/smll.202309387

R. Cugat, M. Garcia-Batlletbó, P. Laiz
Instituto Cugat, Hospital Quironsalud Barcelona, Spain
Fundación García Cugat
Barcelona 08023, Spain

J. M. Carrillo
Bioregenerative Medicine and Applied Surgery Research Group, Department of Animal Medicine and Surgery, CEU Cardenal Herrera University, CEU Universities, Valencia, Spain. García Cugat Foundation CEU-UCH Chair of Medicine and Regenerative Surgery, CEU Cardenal Herrera University
CEU Universities
Valencia 46115, Spain

T. Patiño
Department of Biomedical Engineering, Institute for Complex Molecular Systems (ICMS)
Eindhoven University of Technology
Eindhoven 5612 AZ, The Netherlands

S. Sánchez
Institució Catalana de Recerca i Estudies Avancats (ICREA)
Passeig Lluís Companys 23, Barcelona 08010, Spain

including nanopropellers which can move in glycerol and HA,[5,6] or micropropellers able to swim in the porcine vitreous body of the eye,[7] bovine oviduct fluid,[8] or blood.[9] Although magnetic steering is the most extended method involving micro and nanomotors to guide them in viscous fluids, other alternatives are emerging recently including acoustic control,[10] light-driven Janus NMs,[11,12] and autonomous motion of algae-nanoparticle hybrid microrobots.[13]

Regarding micro- and nanomotors internally driven, chemical[14,15] and enzyme-powered NMs[16,17] are considered excellent candidates since they obtain the energy to self-propel from chemical or catalytic reactions. An intriguing strategy involves the creation of MnO_2-nanomotors for the purpose of active rheumatoid arthritis therapy.[18] While this innovative material shows promise, its reliance on peroxide raises concerns about potential impacts on cell viability. Moreover, the present study has concentrated on the analysis of NM mobility in aqueous surroundings, extending up to 10 mM H_2O_2. Given the absence of molecular weight information regarding HA in the work, the potential for this material to exhibit collective movement within intricate environments remains uncertain. Another approach demonstrated the use of urease-coated micropropellers to penetrate mucin gels using a propulsion combining external magnetic guidance with enzymatic catalysis.[19] Choi et al.[20] presented a self-propelled urease-powered polydopamine micromotor that penetrated deep into the gastrointestinal tract, indicating potential for oral drug delivery. More recently, the enzymatic degradation of surrounding media has been explored to enhance the NMs' penetration into complex environments. For instance, collagenase-based enzymatic micromotors have been used for enhanced tissue penetration in collagen fiber networks that mimic ECM.[21,22] In assisted reproduction, where the cumulus cells constitute a highly viscous media, researchers have developed 4D-printed sperm-hybrid microcarriers that contain hyaluronidase to help sperm cells digest cumulus cells, the final barrier to fertilization.[23]

Up to date, the use of enzymatic propulsion of NMs is gaining special interest. Novel materials are exploring the possibility of combining two enzymes in the same chassis, with the aim of harnessing the advantages offered by both catalytic reactions.[24] While hyaluronidase serves to reduce the viscosity within the tumor region, urease facilitates the self-propulsion of the NM, thereby enhancing the diffusion of the therapeutic agent in the tumor tissue. Although the integration of both enzymes in the same chassis to address the issue of viscosity seems an attractive approach, the basic conditions produced by the urease may diminish the enzymatic activity of hyaluronidase, which could pose a limitation.

Our group has recently made significant discoveries in the field of enzyme-powered NMs, focusing on the use of swarms to improve collective displacement in vivo[25] or the mechanical disruption of extracellular barriers by using a tandem of NMs.[26] Based on these findings, our work aims to study how NMs can overcome biological barriers by modulating viscous media while maintaining continuous propulsion in the surrounding environment.

In this work, we introduce an engineering system composed of "troops" of enzyme-NMs acting one after the other. The first troop (Troop 1) is based on hyaluronidase NMs (HyaNMs) and interacts with the SF by reducing its viscosity. The second troop (Troop 2) is based on urease NMs (UrNMs) and exhibits a collective (swarm-like) behavior while swimming through the viscous media, leading to the improved diffusion of macromolecules as a result of fluid mixing. What we propose here is a system engineering that allows a variety of "second troops" to be delivered on demand independently of the first enzyme used. By using the second troop as an active principle vehicle (like growth factors, for instance) enables their translation approach, regulatory and patenting affairs.

2. Experimental Section

Ethanol (EtOH, 99%), methanol (MeOH, 99%), hydrochloric acid (HCl, 37%), tetraethylorthosilicate (TEOS, 99%), triethanolamine (TEOA, 99%), cetyltrimethylammonium bromide (CTAB, 99%), 3-aminopropyltriethoxysilane (APTES, 99%), glutaraldehyde (GA, 25% in water), hyaluronidase (from bovine testes, type VIII, lyophilized powder, 300–1000 units mg^{-1} of solid), urease (from *Canavalia ensiformis*, type IX, powder, 50 000−100 000 units per gram of solid), bovine serum albumin (BSA,≥ 98%), urea (99.9%), hyaluronic acid sodium salt (HA, from *Streptococcus equi*, with an average molecular weight between 1.5 and 1.8 × 10^3 kDa), sodium chloride (NaCl), potassium chloride anhydrous (KCl), sodium phosphate monobasic (NaH_2PO_4), and sodium phosphate dibasic (Na_2HPO_4), fluorescein isothiocyanate-dextran (10 kDa, FD10), fluorescein isothiocyanate-dextran (70 kDa, FD70), phenolsulfonphthalein (Phenol Red) were purchased from Merck. All reagents were used as received without any further purification. Pierce BCA Protein Assay Kit and phosphate-buffered saline (PBS) were purchased from Thermo Fisher. The water used for the experiments was of type I ultrapure quality, obtained from a purification system (18.2 MΩ cm). Synovial fluid from sheep was provided by Hospital Clínico Veterinario at the University Cardenal Herrera (Valencia) and by Bellvitge Animal Experimentation Unit at the Scientific and Technological Centers of the University of Barcelona. Since the animals were slaughtered before physiological SF acquisition, no ethical permission was required.

2.1. Synthesis

2.1.1. Synthesis of Mesoporous Silica Nanoparticles (MSNP)

Mesoporous silica nanoparticles (MSNPs) with an average diameter of 450 nm were synthesized following a sol–gel process based on the Stöber method, with some modifications.[27] Briefly, a solution of CTAB (570 mg) and TEOS (35 g) in MilliQ-water (20 mL) was heated to 95 °C in a silicon oil bath, using a three-neck round-bottom flask under reflux and constant stirring for 30 min. After homogenization, TEOS (1.5 mL) was added dropwise using a Pasteur pipette. The reaction was left for 2 h under the same conditions of reflux, temperature, and stirring. Then, the resulting silica NPs were collected by centrifugation (1350 g, 5 min).

MSNPs were created using an acidic MeOH solution under reflux to remove the CTAB. For this, MSNPs were suspended in

MeOH (30 mL) adding hydrochloric acid (1.8 mL). The mixture was placed in a one-mouthed round-bottom flask in a silicon oil bath at 80 °C for 15 h. Finally, the resulting MSNPs were collected by centrifugation (1350 g, 5 min) and washed three times in EtOH, sonicating for 10 min between each centrifugation. The final concentration of MSNPs obtained was calculated by dry weighing.

2.1.2. Amine Modification of Mesoporous Silica Nanoparticles (MSNP–NH_2)

MSNPs were functionalized with APTES to modify their surface with primary amine groups (MSNP–NH_2). Briefly, APTES (6 µL mL^{-1}) was added to a suspension of MSNPs (1 mg mL^{-1}) in 70% EtOH solution. The mixture was heated to 70 °C in a silica oil bath while stirring for 1 h. In the following step, MSNP–NH_2 were collected by centrifugation and washed in EtOH (three times, 1150 g, 5 min) and in ultrapure water (three times, 1500 g, 5 min) with vortexing for 30 s and sonicating for 10 min between each centrifugation.

2.1.3. Nanomotor Fabrication (HyaNMs, UrNMs, and MSNP–BSA)

NMs were fabricated using GA as a linker molecule between primary amino groups and proteins, enabling covalent binding. For this, MSNP–NH_2 (900 µL, 1 mg mL^{-1} in PBS 1×) were activated by adding GA (100 µL). The mixture was reacted for 2 h at room temperature while mixing in a rotary shaker. Then, the particles were collected by centrifugation and washed in PBS 1× (three times, 1150 g, 5 min), vortexing for 30 s, and sonicating for 10 min between each centrifugation. Finally, the GA–MSNP were resuspended in a solution of PBS 1× containing hyaluronidase (2 mg mL^{-1}), urease (3 mg mL^{-1}), or BSA (3 mg mL^{-1}) to obtain HyaNMs, UrNMs, or MSNP–BSA, respectively. The mixture was placed on a rotary shaker and kept at room temperature overnight. The resulting NMs were collected by centrifugation and washed with PBS 1× (three times, 1150 g, 5 min), vortexing for 30 s between each centrifugation. The amount of attached protein was quantified using a BCA Protein Assay Kit by measuring the absorbance at 562 nm of each supernatant in an Infinite M200 PRO Multimode Microplate Reader.

2.1.4. Simulated Synovial Fluid

Simulated synovial fluid (SSF) was prepared according to the literature with minor modifications,[28–30] namely mixing a solution containing HA (6 mg mL^{-1}), potassium chloride (5.4 mM), sodium chloride (274 mM), disodium phosphate (20 mM), and potassium dihydrogen phosphate (3.6 mM) and adjusting pH to 7.4.

2.2. Physicochemical Characterization

2.2.1. Hydrodynamic Radii and Surface Charge

Hydrodynamic radii and surface charge were determined by dynamic light scattering (DLS). Hydrodynamic radii were measured using a Wyatt Möbius coupled with an Atlas cell pressurization system. Surface charges were measured with a Malvern Zetasizer. All measurements took place at 25 °C and the light scattering was detected at 173°.

2.2.2. Enzymatic Activity in Simulated Synovial Fluid

The urease activity either in free solution or attached to the MSNP surface was evaluated in the presence of different concentrations of urea. Phenol red, a pH indicator that transitions from yellow to magenta at pH values between 6.6 and 8.2, was used to monitor the increase in pH resulting from the production of ammonia during urea hydrolysis. We tested the enzymatic activity in three conditions: 1) aqueous media (PBS 1×), 2) HA at 3 mg mL^{-1}, and 3) HA at 2 mg mL^{-1}, both in PBS. The last one matched the viscosities achieved after HyaNMs pretreatment in SSF.

We prepared urea solutions with varying concentrations (0, 50, 100, and 200 mM) in aqueous media or in SSF, adding phenol red indicator (0.04% w/w). Then, 2 µL of PBS (blank), UrNMs (1 mg mL^{-1}), or free urease (100 µg mL^{-1}) was mixed with 200 µL of urea solutions. The enzymatic activity was analyzed over time by measuring the absorbance at 560 nm of each well in an Infinite M200 PRO Multimode Microplate Reader.

2.2.3. Scanning and Transmission Electron Microscopy

Scanning electron microscopy (SEM) images were captured by an FEI NOVA NanoSEM 230 at 5 kV. TEM images were captured using a JEOL JEM-2100 microscope at 200 kV. The posterior data analysis was performed with the software Image J (v.1.53).

2.2.4. Sample Sputtering to Enhance SEM Observation

Using a Leica EM ACE600 sputter coater, all the samples were sputtered with Au prior to SEM observation to enhance the conductivity and therefore, the resolution and contrast. The settings were: working distance of 45 mm and current strength of 30 mA, which led to a 10 nm thick coating of sputtered Au after 2 min of atom exposure.

2.3. Rheological Characterization

Rheological measurements of simulated and ex vivo synovial fluid were performed using the MCR 702 rheometer from Anton Paar, coupled with a cone plate of 40 mm diameter, CP40-1, no. 2627. This cone had a fixed working gap of 0.078 mm. All measurements took place on 350 µL of sample and at a constant temperature of 37 ± 0.2 °C. All measurements were carried out in triplicate, keeping the average values. Flow curves were measured with a logarithmic ramp of shear rate for values between 1 to 100 s^{-1}. Oscillation tests to determine the storage (G') and loss (G'') modulus were conducted using a time sweep procedure at constant shear stress of 1 Pa and angular frequency of 10 rad s^{-1} for 4 h.

2.4. Diffusion Analysis of Fluorescein Isothiocyanate-Dextran in SSF

Optical videos of the diffusion of FD10 and FD70 in SSF were recorded on a Hamamatsu camera attached to a Leica DMi8 inverted fluorescence microscope equipped with a 1.25× objective. For this, FD10 or FD70 (3 µL, 2 mg mL^{-1} in PBS 1×) were placed in a Petri dish, filled with SSF (3 mL) without or with HyaNM (250 µg mL^{-1}) pretreatment for 4 h. Videos were recorded for 110 s at 1 frame s^{-1} (FPS), the microscope's maximum capture rate when both fluorescence and optical pictures need to be captured. Videos were analyzed with the software ImageJ (v.1.53) to quantify the areal coverage of FD10 and FD70 in the SSF.

2.5. Motion Studies

2.5.1. UrNM Single Particle Tracking and Mean Squared Displacement (MSD) Analysis

A Leica DMi8 inverted optical microscope equipped with a 63× water objective to observe and record the motion of the nanomotors was used. The nanomotors were suspended in an aqueous solution of UrNMs, which was mixed with HA and urea at the desired concentrations. We prepared a PDMS well with a hole, covering a glass slide, where we placed the mixture solution. To prevent artifacts caused by the drifting effect, we covered the mixture with a coverslip. We recorded videos of 30 s duration for the first 2 min after mixing to ensure that the analysis was performed under consistent conditions. The videos were recorded at a frame rate of 50 FPS, using a Hamamatsu camera in bright field mode. To obtain the tracking trajectories, we analyzed the videos using a custom-made Python code. Next, we calculated the mean squared displacement (MSD) using the following **Equation 1**:

$$MSD\ (\Delta t) = \left\langle x_i\,(t+\Delta t) - x_i\,(t)\right)^2 \Big\rangle \tag{1}$$

The diffusion coefficient (D_e) was obtained by fitting the data to Equation 1 which is applicable for small particles with low rotational diffusion at small time intervals. We analyzed eight particles per condition to determine the resulting D_e, and the error was calculated as the standard error of the mean (SE).

2.5.2. UrNM Swarming Behavior

Optical videos of the UrNM swarms were recorded on a Hamamatsu camera attached to a Leica DMi8 inverted fluorescence microscope equipped with a 1.25× objective. For this, UrNMs (3 µL, 10 mg mL^{-1} in PBS 1×) were placed in a Petri dish, filled with SSF (3 mL) without or with HyaNM (250 µg mL^{-1}) pretreatment for 4 h. Videos were recorded for 110 s at 17 FPS in SSF.

For videos of UrNM swarms mixed with FD10 or FD70, 3 µL of a mixture containing UrNMs (10 mg mL^{-1} in PBS 1×) and FD10 or FD70 (2 mg mL^{-1}) were suspended in PBS 1× and placed in a Petri dish, filled with SSF (3 mL) without or with HyaNM (250 µg mL^{-1}) pretreatment for 4 h. Videos were recorded for 110 s at 1 FPS (maximum capture rate, see previous section). Both videos were analyzed with the software ImageJ (v.1.53) to quantify the areal coverage of UrNMs in the SSF.

Videos in ex vivo synovial fluid were recorded using a custom-built polydimethylsiloxane (PDMS) well, designed using AutoCAD (v. 2019), exported as .stl files, and transformed to GCode for printing on a Cellink Inkredible+ 3D bioprinter. PDMS at a ratio of 1:20 was cured at 65 °C for at least 5 h. Then, 180 µL of ex vivo synovial fluid was placed into the well before adding 2 µL of a mixture containing UrNMs (10 mg mL^{-1} in PBS 1x) and FD70 (2 mg mL^{-1}). Videos were recorded following the same procedure as described above for fluorescence videos.

2.5.3. Computational Analysis of the Swarms

Videos were resized from 2048 × 2048 to 1024 × 1024 px and down-sampled to 1.7 FPS to reduce subsequent calculation time. The background was subtracted based on the average intensity of the area covered by the NMs in the first video frame. The ex vivo videos were not resized but kept at the original size of 2048 × 2048 px (1 FPS). The background was subtracted by using the green channel of the first frame. Then, the videos were corrected for light inhomogeneities and contaminations from the microscope lens or the sample. Pixel intensities were summed along the video frames' x- and y-directions. For instance, the pixel intensity along the y-th row was calculated using the following Equation 2:

$$\bar{I}_y = \frac{1}{N_x}\sum_{n=1}^{N_x} I_{n,y} \tag{2}$$

where, N_x is the total number of pixels in a row and I is the pixel intensity. The y-projection reads accordingly. The projections were then evaluated for all the frames. The normalized intensities were calculated for all video frames.

The area covered by NMs was calculated by converting the video frames into binary images, using a threshold of 5% of the maximum intensity by following Equation 3:

$$I_n^{bi} = \begin{cases} 1 \text{ if } I > 0.05\ I_n \\ 0 \text{ else} \end{cases} \tag{3}$$

The area was defined as the sum of these binary intensities (Equation 4):

$$A = \sum_{n=1}^{N} I_n^{bi} \tag{4}$$

Changes in area over time were calculated as the difference between the area at time t, A(t), and at time 0, A0, using the following Equation 5:

$$\Delta A\ (t) = A\,(t) - A_0 \tag{5}$$

All computational analyses were performed in Matlab (v. R2022a, Mathworks, Inc., USA).

3. Results and Discussion

3.1. Fabrication and Characterization of Enzyme-Powered Nanomotors

NMs based on MSNPs were fabricated using sol-gel chemistry based on the Stöber method with some modifications.[27]

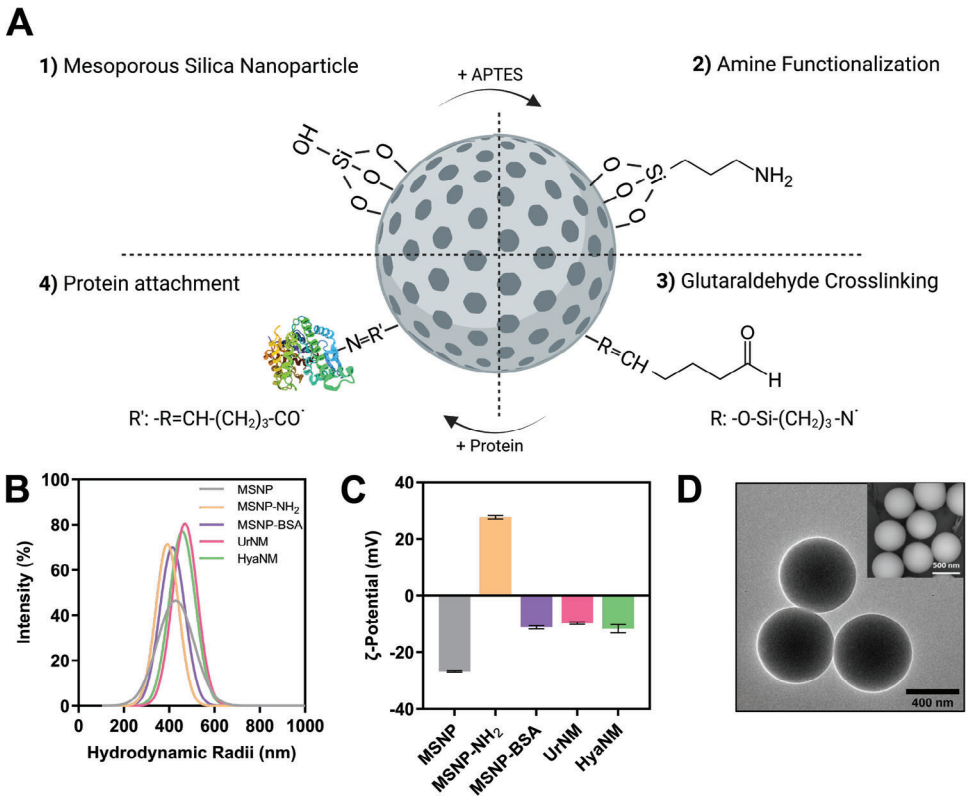

Figure 1. Fabrication and characterization of enzyme-powered NMs. A) Scheme showing the stepwise process to fabricate the NMs. B) Hydrodynamic radii and C) Surface charge characterization of MSNPs and the subsequent stepwise modifications to obtain NMs. ($N = 3$, results are shown as mean ± SE). D) TEM image of mesoporous silica nanoparticles (MSNPs). Scale bar: 400 nm. Inset: SEM image of MSNPs size distribution. Scale bar: 500 nm.

Their surface was chemically functionalized with primary amino groups by linking 3-aminopropyltriethoxysilane (APTES). Then, the amino groups were activated using GA as a crosslinking agent. This enabled the covalent binding between the MSNPs and the enzyme, leading to the establishment of an asymmetric distribution. The introduction of GA through chemical functionalization has been reported to generate asymmetric patches on the surface of MSNPs, resulting in a nonhomogeneous and random distribution of enzymes.[31,32] This uneven enzyme distribution can generate a stochastic propulsive force, which ultimately drives the motion of NMs. Subsequently, after the addition of GA, the protein was covalently attached to the surface (**Figure 1A**). This methodology was replicated using different proteins (urease, hyaluronidase, and bovine serum albumin) to prepare all the materials used in this work.

The NM fabrication process was monitored using different techniques. The hydrodynamic radii of the MSNP-based materials were characterized by dynamic light scattering (DLS) analysis (Figure 1B). The DLS characterization on the resulting MSNP showed a broad population, which is in concordance with the poor solubility of silica in water once the surfactant has been removed. However, the hydrodynamic radii distribution corresponding to MSNP–NH_2 showed a narrower peak, suggesting that the presence of free amino groups on the surface increased the stability of the NPs in solution and improved their solubility.[33] For MSNP–BSA, UrNMs, and HyaNMs, single peak populations showed well-dispersed NMs suspension. NMs showed a narrower distribution, confirming that protein attachment did not induce aggregation. Moreover, the NMs exhibit slightly larger hydrodynamic radii, indicating the presence of conjugated enzymes in the MSNPs.

The surface charge (*z*-potential) after each functionalization step was also characterized using DLS (Figure 1C). Surface charges for MSNPs had a value of −26.8 ± 0.3 mV in ultra-pure water, typical for MSNPs. After grafting the NH_2 groups onto the surface, the *z*-potential became positive yielding +27.7 ± 0.6 mV, confirming successful attachment of the free amino groups to the surface. After protein binding, surface charges became negative confirming the successful attachment of BSA (−11.2 ± 0.3 mV), urease (−9.6 ± 0.4 mV), and hyaluronidase (−11.7 ± 0.8 mV), which were in agreement with the isoelectric values of the proteins.[34–36] In addition to the *z*-potential becoming negative, enzyme attachment was also confirmed using a BCA kit assay that quantifies the amount of attached proteins from the reduction of copper by the proteins' peptide bonds. The amount of protein attached was 90.9 ± 0.8 and 184.5 ± 14.8 mg mL^{-1} for urease and hyaluronidase NMs, respectively (Figure S1, Supporting Information) ($N = 3$, results are shown as mean ± SD). We analyzed the enzymatic activity of urease, whether it was free or attached to the surface of MSNP in SSF. Two specific cases were considered: 1) without HyaNMs pretreatment (with enzymatic activity 5.06E + 3 μmol s^{-1} and specific activity 2.81E + 5 μmo s^{-1}

m) and 2) with HyaNMs pretreatment (with enzymatic activity 6.33×10^3 mol s^{-1} and specific activity 3.51×10^3 mol s^{-1} m), with varying concentrations of urea. In the latter case, we used an SSF solution that matched the viscosity achieved through post-HyaNMs pretreatment, instead of directly applying HyaNMs to the SSF. This approach was adopted to prevent particle interference during the measurements. To simplify the discussion, we will refer to these scenarios as "untreated" and "treated" SSF, respectively (Figure S2, Supporting Information). Notable differences were observed between the conditions in terms of the time required to reach the plateau. It took approximately 15 min for the untreated SSF to achieve the plateau, whereas the treated SSF reached the same values in just 10 min. These differences can be attributed to the viscosity of the media. The lower viscosity of the SSF appears to enhance the diffusion of the products released by the enzymatic reaction, resulting in a shorter time required to reach the same values.

The pore structure and morphology of the resulting MSNPs were evaluated by TEM and SEM which provided visual images of the radial pores (Figure 1D) and yielded an average MSNP diameter of 439.6 ± 32.1 nm, revealing the expected highly monodisperse particles.

3.2. Synergistic Effects of Two Nanomotor Troops for Moving Through Complex Media

A majority of studies on the actuation mechanism of self-propelled NMs have focused on liquids such as water or PBS, although most of the fluids present in the human body are considerably more viscous and complex (e.g., biopolymers) which constitute a biological barrier for NMs.[37] It has been reported that enzymatic urease-based NMs mimic the behavior of *Helicobacter pylori*, in that they liquify the viscous medium by increasing the local pH and generating the gel-sol transition.[38] The ammonia released as a product of the catalytic reaction of urease introduces rheological, effectively decreasing the medium's viscosity by breaking internal hydrogen bonds in the polymeric network.[39,40]

SF is a biologically complex medium found in the joints[41] that consists of a viscoelastic fluid that lubricates the joints during movement.[42] Since real SF is difficult to obtain and utilization of animals is required, we propose to use simulated SF (SSF) that mimics this biofluid, particularly its rheological properties. To assess the chemical environment and composition of SSF with HA as the principal macromolecule, we prepared an aqueous solution of HA (3 mg mL^{-1}) following the reported literature.[43]

Changes in HA bulk viscosity, as a result of the collective actuation of the UrNMs, were analyzed by rheology adding UrNMs in different concentrations (10, 50, 100, and 250 µg mL^{-1}) to the HA solution, which contained either 0 or 200 mM of urea (**Figure 2A**). HA is a non-Newtonian viscoelastic fluid with a classic shear thinning behavior, i.e., viscosity decreases under increasing shear strain[44] (Figure 2B i). We observed a significant reduction in bulk viscosity when UrNMs were added to the fluid with urea. To investigate the effect of changing UrNM concentrations in more detail, we analyzed at a constant shear rate of 1 s^{-1} (Figure 2B ii), which corresponds to the physiological frequency experienced by a knee when a person is walking.[45] We observed that the viscosity continuously decreased as the concentration of UrNMs was increased, from 274.9 ± 0.4 (for HA serving as control) to 46.0 ± 1.7 mPa s (with 250 µg mL^{-1} of UrNMs), which corresponds to an 83% reduction. Changes in the rheological properties of HA were attributed to the strong increase in pH due to the ammonia released, leading to the breaking of the hydrogen bonds between the HA chains.[46]

Although HA is the main constituent of SF, the aqueous solution used for the experiments in the previous section did not include salts. However, in SF, this polymer is surrounded by ions that can influence its conformation. In fact, it has been reported that the presence of ions has a considerable effect on the rheological properties of HA solutions.[47,48] To corroborate this, we followed the same rheological protocol using SSF, which is composed of HA and physiological salts. SSF exhibited the same shear thinning behavior as HA in aqueous medium (Figure 2C i). However, the presence of UrNMs only led to slight reductions in viscosity (Figure 2C ii) which stands in rather stark contrast to our findings with HA (Figure 2B ii) although the pH was increased to 9.

Based on previous studies showing that the presence of sodium ions contributes to conformational changes in the HA structure.[49] We had attributed the fact that the viscosity of SSF did not decrease in the presence of UrNMs to chain conformations in this fluid. In fact, HA chains have various carboxylate groups that act as both donors and acceptors of hydrogen bonds. These bonds can be created between HA chains and the surrounding medium. However, when the concentration of salts increases, the number of hydrogen bonds decreases by weakening the swollen standard configuration, thereby increasing the flexibility of the chain. In fact, the number of hydrogen bonds that HA chains can form with water decreases dramatically, which modifies the conformation of the 3D structure and solvates the molecule. Moreover, these sodium ions change the distance between polar groups, which play a key role in the formation of temporary hairpin-like loops, which further promote the flexibility of the chain.[50,51] Overall, these effects decrease the viscosity of the HA, which explains why the presence of UrNMs did not lead to any significant reduction in SSF viscosity.

To overcome these issues, we present a synergistic strategy that combines two types of NMs to reduce SSF viscosity and facilitate better NM penetration. The first troop consists of HyaNMs (Troop 1) and depolymerizes the SSF allowing the second troop consisting of UrNMs (Troop 2) to swim more easily through the viscous medium (**Figure 3A**). This approach takes advantage of the fact that hyaluronidase can cut HA chains, the main component of SSF, into two monosaccharide fragments of lower molecular weight which, and this is our hypothesis, should reduce the viscosity of the medium.[52] To test this hypothesis, we investigated the viscosity of SSF at varying shear rates (from 1 to 100 s^{-1}) after exposing the medium to different concentrations of HyaNMs for 4 h. The results clearly show that the viscosity of SSF decreased as the HyaNM concentration was increased (Figure 3B i). Using a constant shear rate of 1 s^{-1}, the SSF viscosity decreased by 24% from 50 to 38 mPa s as HyaNM concentrations were increased from 10, over 50, to 100 µg mL^{-1}, although this decrease was not statistically significant (Figure 3B ii). Only once the HyaNM concentration was increased further to 250 µg mL^{-1},

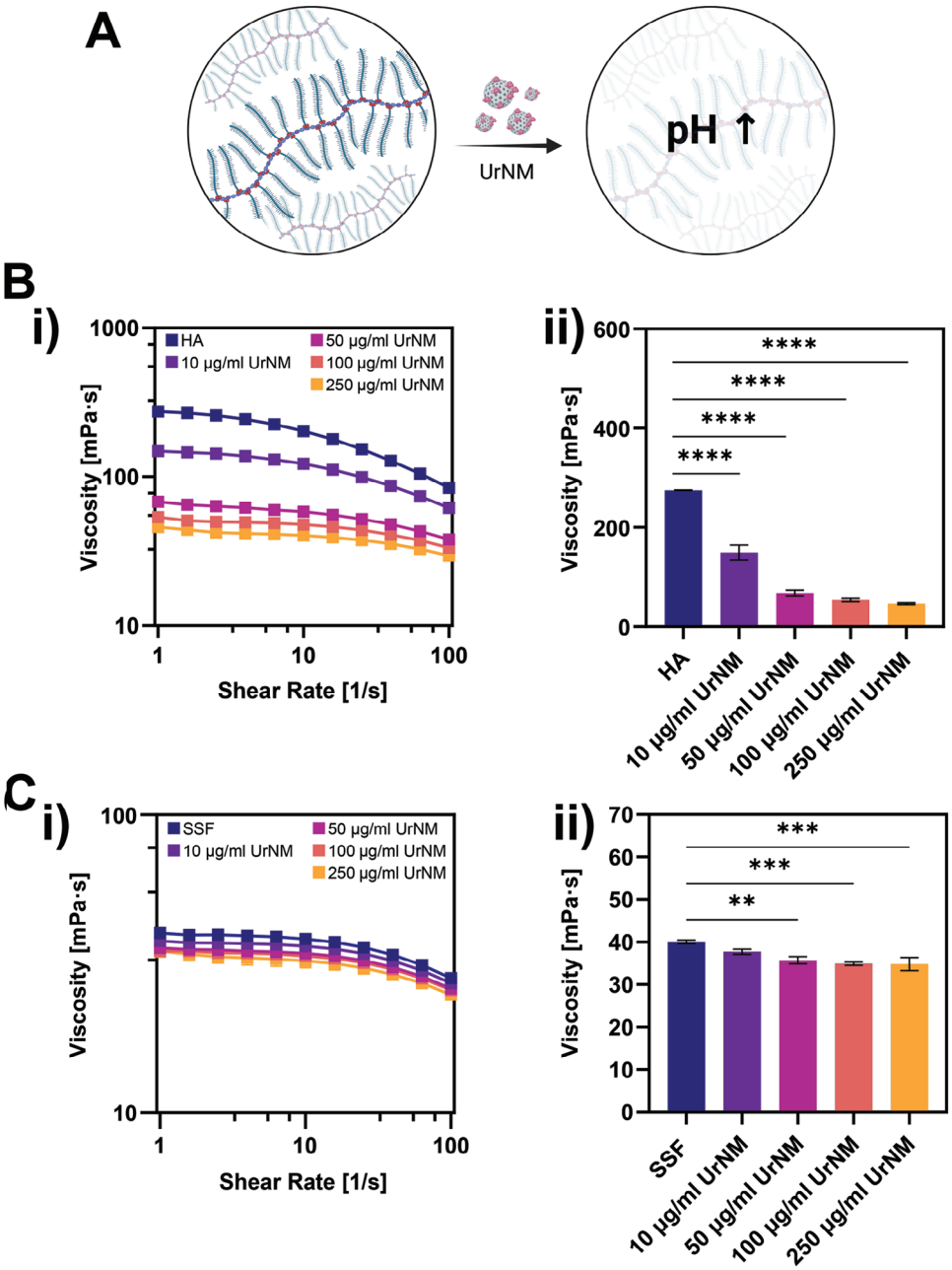

Figure 2. Understanding the influence of salts on the viscosity of HA solutions. A) Schematic illustration of our approach of using UrNMs as possible candidates to move through complex media. B) (i) Viscosity versus shear rate of HA solution after 4 h of exposure to UrNMs in 200 mM of urea and (ii) as in (i) but for a constant shear rate of 1 s^{-1}. C) As in (B) but using SSF ($N = 3$, results are shown as mean ± SE). Asterisks denote a significant difference from the control (being the control HA column for (B) and SSF column for (C)), with: $^{**}p \leq 0.01$, $^{***}p \leq 0.001$, $^{****}p \leq 0.0001$.

did the SSF viscosity show a statistically significant decrease of 48% to 26 mPa s.

To study the controlled depolymerization of SSF mediated by the HyaNMs in more detail, we monitored the storage modulus (G', solid behavior) and loss modulus (G'', liquid behavior) over the 4 h exposure to HyaNMs while applying a constant shear stress of 1 Pa and an angular frequency of 10 rad s (Figure 3C). The results show that both SSF moduli remained nearly constant throughout the experiment. Only once the SSF was treated with HyaNMs (250 μg mL^{-1}) did both moduli decrease continuously over time in a sustained manner. After 4 h, the solid modulus had decreased by 98% from 58 to 1.27 mPa s and the liquid component by 71% from 450 to 130 mPa s. It is also important to note that we observed considerable fluctuations in the measurements from about 160 min onward, possibly due to the solid modulus dropping to near our equipment's detection limit. As a control, we also analyzed the moduli of SSF in the presence of free hyaluronidase and MSNP–BSA, i.e., passive NMs. Free

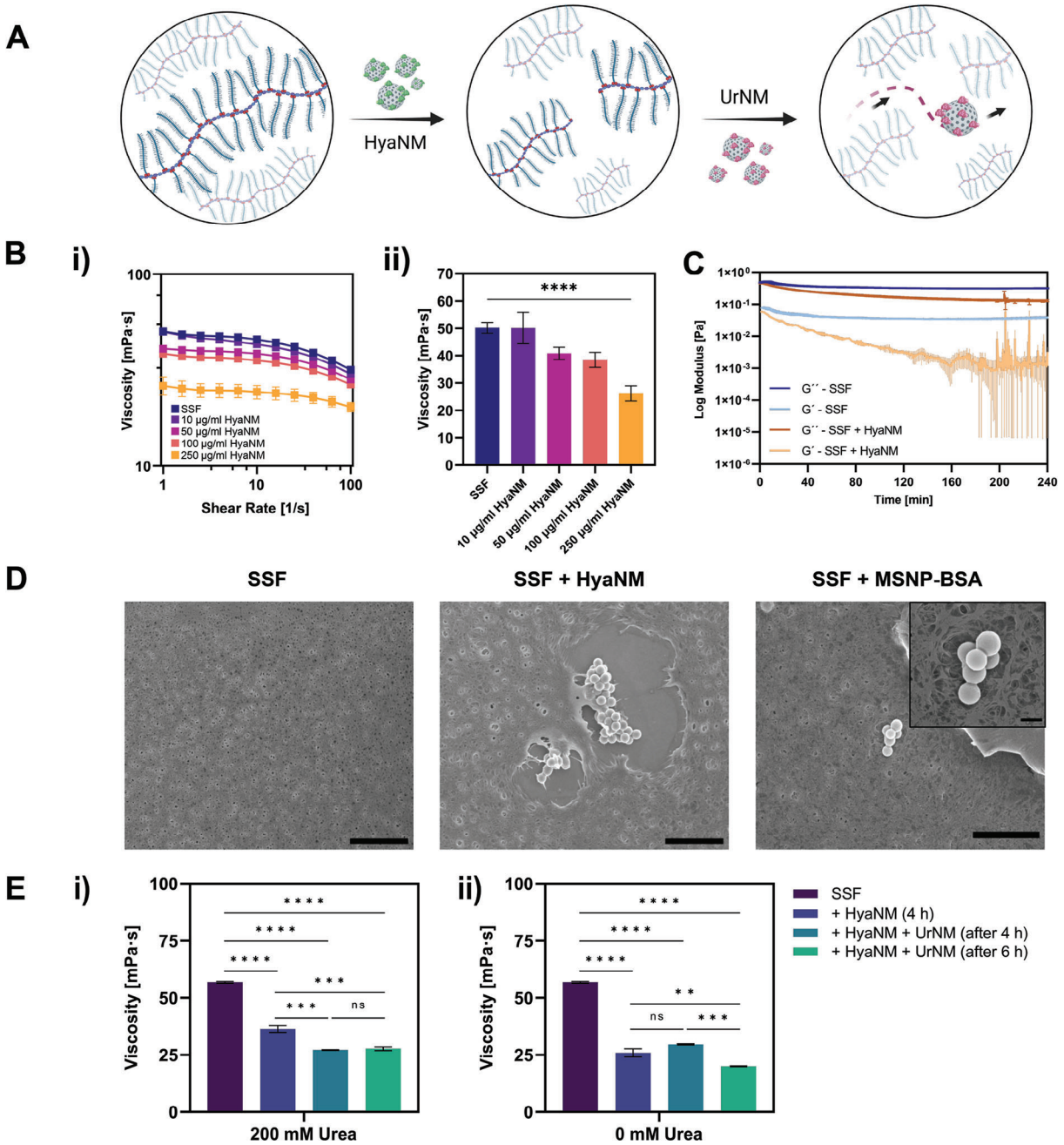

Figure 3. Modulating the viscoelastic properties of SSF through the combined actuation of HyaNM and UrNM troops. A) Scheme illustrating the approach of using HyaNMs as a first troop to decrease SSF viscosity, allowing the second troop of UrNMs to swim more easily through the fluid. B) (i) SSF viscosity versus shear rate and (ii) SSF viscosity at a constant shear rate of 1 s^{-1} at different concentrations of HyaNMs ($N = 3$, results are shown as mean ± SE). Asterisks denote a significant difference from the control (being the control SSF column) with $^{****}p \leq 0.0001$. C) Evolution of the loss and storage moduli of SSF and SSF + HyaNMs (C = 250 µg mL^{-1}) over time. D) SEM images of SSF, SSF + HyaNMs, and SSF + MSNP–BSA (Inset: scale bar = 400 nm). Scale bar = 5 µm. E) SSF viscosity at a shear rate of 1 s^{-1} in the presence of both HyaNM and UrNM troops in i) 200 mM of urea and ii) 0 mM of urea. ($N = 3$, results are shown as mean ± SE). Asterisks denote a significant difference from the control (being the control SSF column) with: $^{**}p \leq 0.01$, $^{***}p \leq 0.001$, $^{****}p \leq 0.0001$.

hyaluronidase caused a total and immediate disruption of the medium which resulted in a significant decrease in both the solid and liquid SSF moduli (Figure S3A, Supporting Information). In contrast, when passive NMs were used instead, the SSF moduli remained nearly unchanged over time (Figure S3B, Supporting Information). This interpretation is further supported by SEM images that clearly show how HyaNMs were able to break the SSF structure, creating holes which in turn led to a decrease in the medium's viscosity (middle panel in Figure 3D). This effect can be also observed in an SEM image offering a broader view

(Figure S4, Supporting Information). The first and third panels in Figure 3D show the structure of the SSF without HyaNMs and in the presence of passive NMs (MSNP–BSA), respectively. Without HyaNMs, the structure appears unaltered without any holes. With passive NMs, although the polymeric structure of the SSF interacts with these NPs, the actual SSF structure also remains intact.

To examine the effect of combining Troops 1 and 2, we characterized the SSF in the presence of urea (200 mM) and a constant shear rate of 1 s^{-1} (Figure 3E i). With this setup, the SSF viscosity decreased by 37% from 57 to 36 mPa s after exposing the medium to HyaNMs (c = 250 μg mL^{-1}) for 4 h. By adding UrNMs, the SSF viscosity immediately decreased by an additional 25% to 27 mPa s. These results are in agreement with other studies that reported a decrease in HA viscosity for lower shear rates and higher pH (e.g., pH 9). The catalytic activity of the UrNMs produces ammonia as a by-product of the catalytic reaction which increases the pH of the ambient medium around to 9. Considering that the optimal pH range for the catalytic activity of hyaluronidase is 6–8, the HyaNM activity will decrease notably when UrNMs have hydrolyzed the urea and increased the pH to 9.[53] We used this effect to our advantage in order to control and stop the reduction in SSF viscosity once the optimal value had been reached. To demonstrate this, the viscosity of the SSF was measured 2 h after adding the UrNMs (total time 6 h) which showed no significant difference to the values obtained immediately after the UrNMs had been added. Without urea, we observed a similar viscosity reduction of 55% from 56 to 25 mPa s after 4 h (Figure 3E ii). However, without urea, the UrNMs were unable to increase the pH of the medium and their presence therefore had no immediate effect on SSF viscosity. The effect only occurred with some delay, as the HyaNMs continued to digest the SSF while the pH was maintained in the physiological range, the viscosity eventually dropped by an additional 35% from 29 to 19 mPa s, 2 h after having added the UrNMs (i.e., after a total time of 6 h). Overall, these results demonstrate that the treatment of SSF with HyaNMs for 4 h was highly effective at decreasing the viscosity of the medium before adding the UrNMs. The UrNMs were able to stop the chemical disruption of the SSF and could move more easily through the complex medium.

3.3. Motion of UrNMs in Simulated Synovial Fluid: Analysis at Single Particle Level and Collective Behavior

The urease NMs catalyze the hydrolysis of urea into ammonia and carbon dioxide in the presence of urea following Equation 6:

$$(NH_2)_2CO + H_2O \rightarrow CO_2 + 2NH_3 \quad (6)$$

Previous studies have reported enhanced diffusion using urease as an enzymatic NMs. In that sense, self-diffusiophoresis mechanism, where the catalytic reaction of enzymes generates a gradient of reaction products around the NMs, is the most studied mechanism to explain the motion of NMs.[54,55]

We analyzed the self-propulsion of urease NMs due to the presence of urea by optically tracking their trajectories containing either 0 and 200 mM of urea in SSF based on two scenarios: 1) SSF without HyaNMs pretreatment, and 2) SSF with the viscosity values achieved with post-HyaNMs pretreatment. For ease of reference, we named these scenarios "untreated" and "treated" SSF, respectively. To assess how post-HyaNMs treatment affected motion analysis at the single-particle level, we utilized a HA solution that fitted the viscosity achieved through HyaNMs pretreatment, instead of applying HyaNMs directly to the SSF. This was done to prevent confusion in particle tracking of UrNMs or HyaNMs. Then, MSD, diffusion coefficient, and trajectories of each condition were evaluated using custom-made Python code. The MSD resulting from the tracked trajectories showed a linear increase with time, indicating diffusive motion. Although a slight and nonsignificant increase of enhanced diffusion was observed in the SSF untreated, a clear difference was noticeable between 0 and 200 mM of urea in the SSF "treated" (**Figure** 4A i).

The effective diffusion coefficient (De) was determined by fitting the MSD curves to the following Equation 7:

$$MSD(\Delta t) = 4D_e\Delta t \quad (7)$$

where Δt represents the time interval.

Regarding the resulting effective D_e obtained, it can be observed that increasing the urea concentration from 0 to 200 mM did not enhance diffusion in SSF "untreated." Both conditions demonstrated solely Brownian motion, as evidenced by their MSDs and their D_e, being indistinguishable between them, possibly due to the relatively high viscosity of the media (Figure 4A ii). By contrast, significant differences in D_e for UrNMs in both SSF "untreated" and "treated," even in the absence of urea, were attributed to an increase in diffusion resulting from Brownian motion due to differences, in terms of viscosity of the media, among the different scenarios. In SSF "treated," UrNMs exhibited a significant increase in self-propulsion at 200 mM urea compared to the absence of the substrate. By increasing the urea concentration up to 200 mM, the D_e increased from 0.0451 ± 0.00183 to 0.0642 ± 0.00522 μm s^{-1}. The resulting data provided direct evidence of UrNMs self-propulsion in viscous media. Representative tracking trajectories of UrNMs for the four conditions are represented in Figure 4B.

Having investigated the effects of two troops of NMs, we examined not only their motion at single particle level, but also their corresponding collective motion in vitro by optical microscopy. The effect of Troop 1 (HyaNMs) was evaluated by comparing how far Troop 2 (UrNMs) was able to diffuse through the untreated and treated SSF. As mentioned above, pretreatment with HyaNMs led to a reduction in SSF viscosity and enhanced UrNM diffusion. The UrNM collective motion dynamics in SSF were investigated by optical microscopy (**Figure** 5A). For this, UrNMs were placed onto a Petri dish, filled with SSF without or with urea, recording their dynamics on video for 110 s. The results were recorded on video for 110 s to visualize the temporal evolution of UrNMs areal coverage (Movie S1, Supporting Information).

Without HyaNM pretreatment, UrNM diffusion was low and most NMs quickly settled onto the bottom of the Petri dish (Figure 5A i). If SFF was pretreated with HyaNMs, UrNM diffusion was higher, and they were able to cover a larger area (Figure 5A ii). In order to obtain a more quantitative measure of UrNM diffusion we analyzed the recorded videos for pixel intensity, area covered, and UrNM velocity, by computational analysis

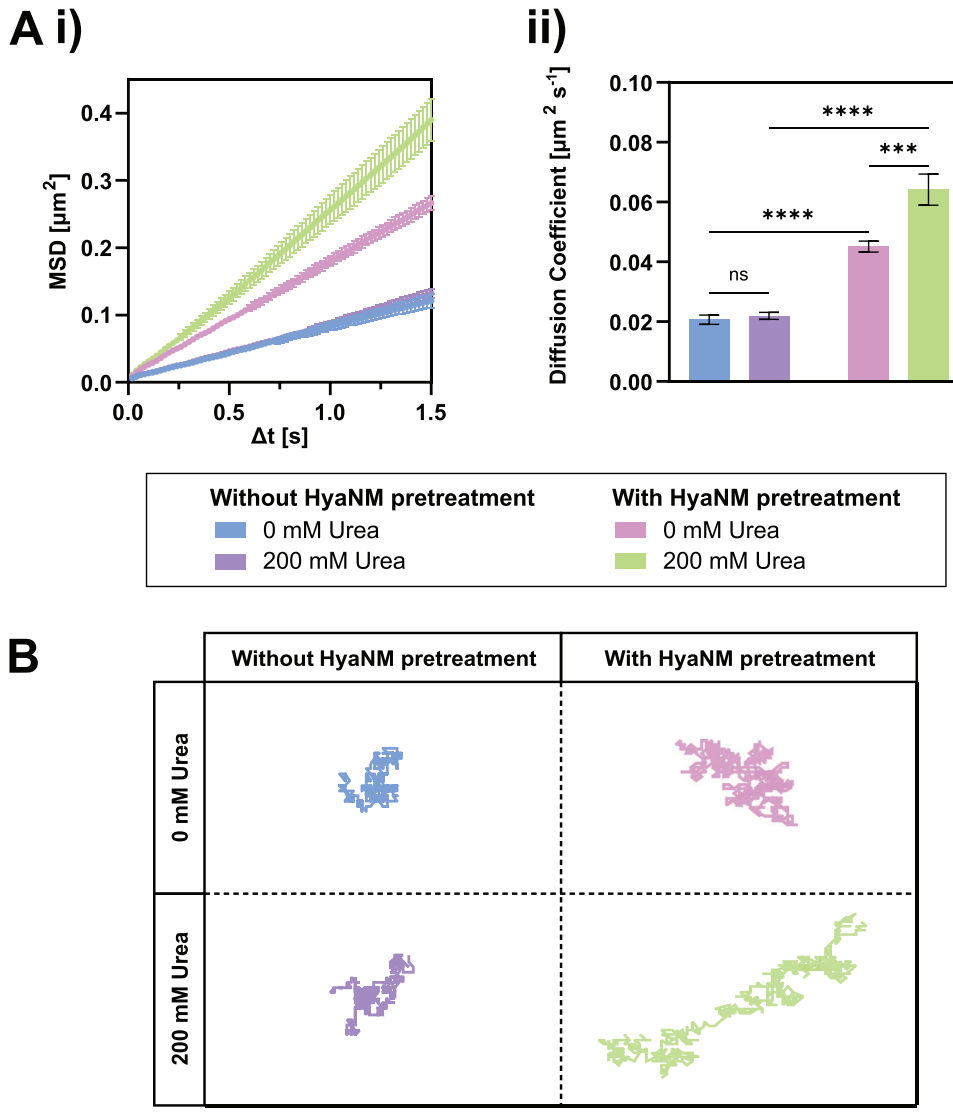

Figure 4. Motion analysis of UrNMs at single particle level in SSF. A) Effective diffusion coefficients obtained by MSD analysis and B) MSDs of UrNMs, in SSF without and with HyaNMs pretreatment, both without and with urea (200 mM). Results are shown as mean ± SE. Asterisks denote a significant difference among conditions with $^{****}p \leq 0.0001$, $N = 8$; C) Representative tracked trajectories of UrNMs, in SSF without and with HyaNMs pretreatment, both without and with urea (200 mM).

using a homemade code (Figure 5B; Movies S2 and S3, Supporting Information).

A comparison of the pixel intensity along a section that cuts through the center of the UrNM particle cloud clearly shows that UrNMs diffuse more easily if the medium has been pretreated with HyaNMs (Figure 5B ii vs i). This also becomes apparent if we consider the spread, i.e., the area covered by UrNMs (Figure 5C). With and without HyaNM pretreatment, the area covered by UrNMs after 110 s has grown by 8.0 and 44.2 mm^2, respectively. Thus, pretreatment with HyaNM led to a 5.6-fold increase in the areal coverage of UrNMs, highlighting the efficiency of HyaNMs at enhancing UrNM diffusion. Moreover, the slope in the pretreated sample shows an increase until about $t = 45$ s from which point it starts to decrease toward an asymptotic limit. These changes are related to changes in areal expansion velocity (Figure 5D), which increases in pretreated samples from ≈0.2 to 0.4 $mm^2\ s^{-1}$ at time $t = 45$s, before starting to decrease. The corresponding results for UrNM diffusion in the absence of urea are shown in Figure S5A (Supporting Information). In these control experiments, UrNMs quickly settled near the seeding point and the low diffusion resulted in stochastic particle distributions (Figure S5B, Supporting Information). In this case, pretreatment with HyaNMs only led to a 2.8-fold increase in areal coverage (Figure S5C, Supporting Information) after 110 s, solely due to a decrease in viscosity as there is no self-propulsion without urea. The area expansion velocities remained low and reached negligible values at 110 s (Figure S5D, Supporting Information).

Comparing the fold changes in effective area coverage between times $t = 0$ and $t = 110$ s, without HyaNMs pretreatment, we obtained a 1.2-fold (± 0.1) and 1.3-fold (± 0.3) increases without

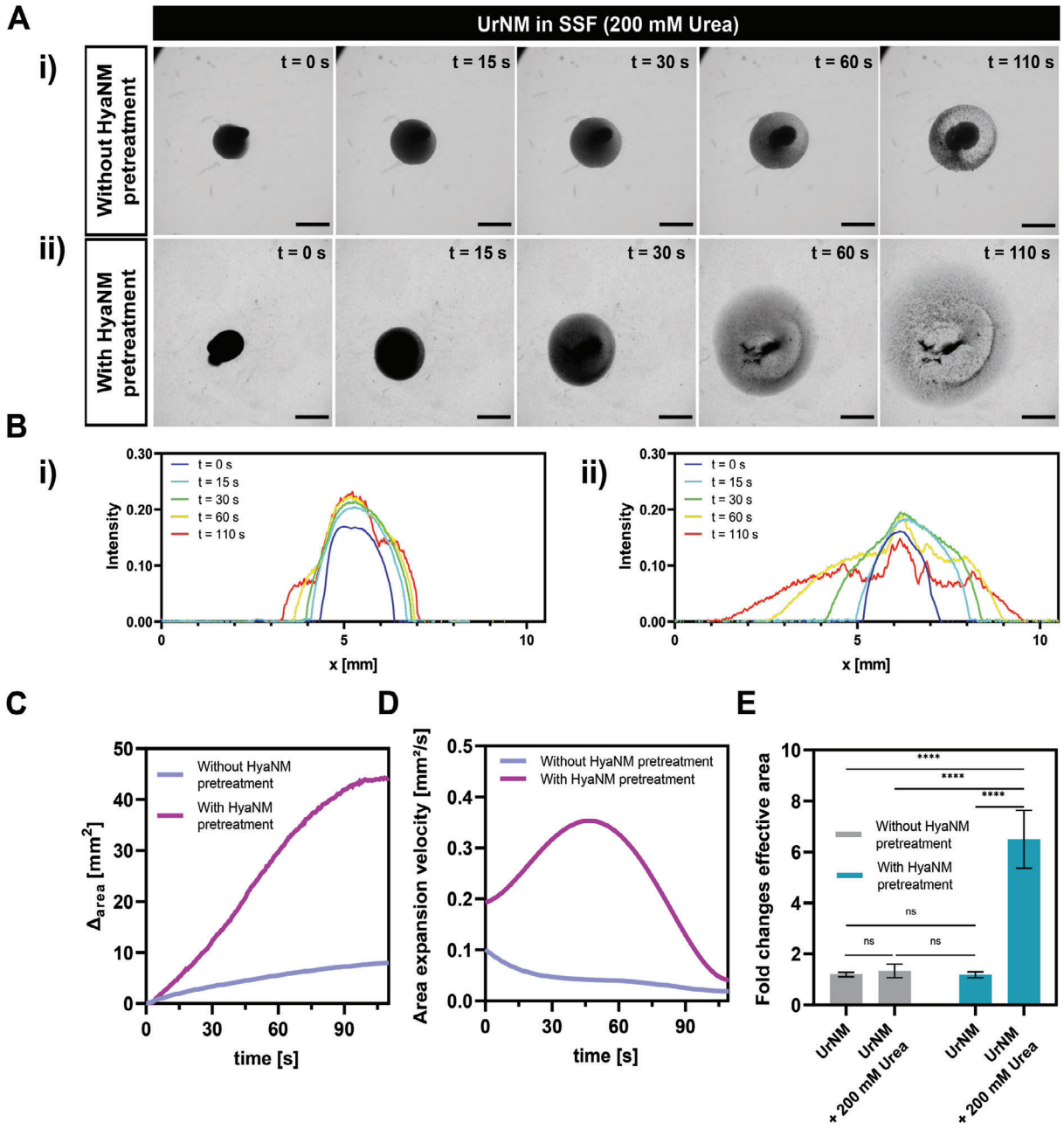

Figure 5. Analysis of UrNM swarming behavior in SSF. A) Video screenshots of UrNMs in SSF with 200 mM of urea i) without and ii) with HyaNM pretreatment at selected time points. Scale bar = 2 mm. B) Projections of the average pixel intensity along the *y*-axis for UrNMs in SFF with 200 mM of urea and i) without and ii) with HyaNMs pretreatment. C) Delta area covered by UrNMs with respect to time 0 s with and without HyaNM pretreatment. D) The area expansion velocity represents the growth in area covered per unit time and is the time derivative of the change in area in panel (C). E) Fold changes in effective area covered by UrNMs between times $t = 0$ and t = 110 s, for SSF with and without HyaNM treatment, and each of those with and without urea ($N = 9$, results are shown as mean ± SE). Asterisks denote a significant difference from the control with $^{****}p \leq 0.0001$.

and with urea (200 mM), respectively (Figure 5E), i.e., statistically identical increases. In contrast, with HyaNM pretreatment the corresponding increases were 1.2-fold (± 0.1) and 6.5-fold (± 1.1), without and with urea (200 mM), respectively. These results can be explained by the Stokes-Einstein equation (Equation 8):

$$D_r = \frac{k_B T}{8\pi\mu r^3} \quad (8)$$

which shows that a liquid's diffusion coefficient is inversely proportional to its viscosity coefficient. These results are also in agreement with our rheological findings which showed that pretreating SSF with HyaNMs led to a decrease in viscosity and allowed UrNMs to diffuse more easily (Figure 3B).

We analyzed the convective flows and buoyancy forces exhibited by UrNMs. To accomplish this, we conducted a series of experiments involving the 3D movement of UrNMs in SSF,

employing a side-view camera for visualization (Figure S6, Supporting Information). Notably, we observed that the introduction of HyaNMs pretreatment played a key role in shaping the buoyant forces within this system. Understanding the buoyancy effect is crucial, especially in fluid environments, as it depends on the density contrast between the NM and the surrounding fluid. Our findings revealed that in the absence of HyaNMs pretreatment, UrNMs exhibited negligible movement in the SSF, regardless of the presence or absence of fuel. It is noteworthy that due to the high viscosity of the medium, the buoyancy effect remained indistinct. However, a significant contrast was observed when the SSF was pretreated with HyaNMs. This pretreatment induced dynamic 3D motion, driven by a combination of forces, including the buoyancy effect and self-propulsion. Despite the viscosity of the SSF remaining higher than that of typical aqueous media, we observed buoyancy effects in the absence of fuel. By contrast, in the presence of fuel, this upward self-propulsion force can be added to the predicted buoyant force of the NMs. The 3D motion of UrNMs was not solely attributed to buoyancy but also originated from the self-propulsion of Troop 2. These insights translate into valuable data, including enhanced velocity profiles and the extent of the area covered, which are shown in Figure S6B (Supporting Information) for scenarios involving the absence of HyaNMs pretreatment of the SSF and in Figure S6C (Supporting Information) for cases where such pretreatment was present.

3.4. Increased Macromolecule Diffusion in Simulated Synovial Fluid Mediated by UrNMs

New treatments based on the application of therapeutic agents such as growth factors (GFs) are becoming increasingly popular to regenerate joint-related diseases.[56] While these novel therapies appear promising, several obstacles such as high medium viscosity still need to be overcome. We propose the use of dextran (as a model molecule that mimics the size of GFs) to combine them with UrNMs in order to increase their diffusion and area coverage. We have used dextran in two molecular weights (10 and 70 kDa), chemically bonded with fluorescein isothiocyanate to facilitate observation (denoted FD10 and FD70, respectively), and we deployed a combination of FD with UrNMs to assess the effect on their diffusion in a complex medium.

The experiments were performed in a mixture of UrNMs and FD10 suspended and placed in a Petri dish, filled with SSF with or without HyaNMs and each of those with and without urea. The diffusing UrNMs and FD10 were recorded on video for 110 s (Movie S4, Supporting Information) via optical fluorescence microscopy. Without urea, diffusion was low and most NMs precipitated at the bottom of the Petri dish (**Figure 6**A i). However, with urea the UrNMs were capable of self-propelled motion and covered a larger area, expanding the reach of FD10 (Figure 6A ii). Pretreatment of SSF with HyaNMs further increased the effective area covered by UrNMs and thus the reach of FD10. Repeating the experiments with FD70 led to similar results (Figure 6B) with no quantitative differences between FD10 and FD70. Looking at fold changes of the effective area between times $t = 0$ and $t = 110$ s, we found that the effective area covered by FD10 in SSF without HyaNMs pretreatment increased 0.8-fold (± 0.2) and 1.5-fold (± 0.2) without and with urea, respectively, although these differences were not statistically significant (Figure 6C i). In contrast, with HyaNM pretreatment, the corresponding increases were 0.7-fold (± 0.1) and 6.1-fold (± 0.6), without and with urea, respectively. Similar results were obtained for FD70 (Figure 6C ii; Movie S5, Supporting Information) with fold changes of 1.4 (± 0.1) and 2.5 (± 0.4), without and with urea, respectively (without HyaNM pretreatment), and 1.8 (± 0.2) and 6.3 (± 0.9), without and with urea, respectively (with HyaNM pretreatment). Thus, no significant differences were found when SSF was or was not pretreated with HyaNMs.

As a control, we evaluated the diffusion of FD10 or FD70 without combining them with UrNMs (Figure S7, Supporting Information). Both FDs showed larger explored areas if SSF was pretreated with HyaNM (Figure S7A, Supporting Information). Without HyaNM pretreatment, the effective area covered by FD10 and FD70 grew 1.5-fold (± 0.1) and 1.6-fold (± 0.2), respectively (Figure S7B, Supporting Information). With HyaNMs pretreatment, the corresponding increases were 3.7-fold (± 0.4) and 2.7-fold (± 0.2) for FD 10 and FD70, respectively.

To clarify the impact of our troop combination on macromolecule diffusion, we examined the changes in FD70 coverage area under various conditions (Figure S7C, Supporting Information). We first looked at FD70 diffusion alone and with HyaNMs, finding no significant difference. This aligns with Figure 3C, showing that HyaNMs' HA chain depolymerization is time dependent. Next, we compared these results to FD70 added to HyaNMs-treated SSF for 4 h, resulting in a slight but statistically insignificant increase in coverage area. This indicates that reducing viscosity alone is not sufficient to boost FD70 coverage. Lastly, when FD70 was co-injected with UrNMs into HyaNMs-pretreated SSF for 4 h, we observed a significant increase in coverage, suggesting UrNMs´ self-propulsion significantly enhances FD70 delivery.

In summary, these results clearly demonstrate how the self-propulsion of UrNMs can greatly increase the diffusion of FD in a viscous medium. Moreover, these increases were independent of the FD's molecular weight, indicating that the nanomotors can guide molecules of different sizes. In other words, our combination of NMs troops will be a promising tool to spread therapeutic agents (e.g., GFs) through the whole joint cavity. Our technology could be promising for the treatment of joint diseases and joint injuries which are commonly managed through the administration of therapeutic agents designed to inhibit the degenerative and inflammatory processes. However, a significant challenge of current approaches is the entrapment of a substantial quantity of therapeutic agents within the viscous joint environment, preventing it from reaching large areas in that confined space. In contrast, our NMs approach has shown remarkable potential for spreading macromolecules within the viscous joint environment thanks to the controlled reduction of the viscosity of the synovial fluid.

3.5. Synergistic Effect of Two NM Troops in Ex Vivo Synovial Fluid

To test whether the promising results obtained in vitro also held up in a more realistic scenario, we studied how combining NMs

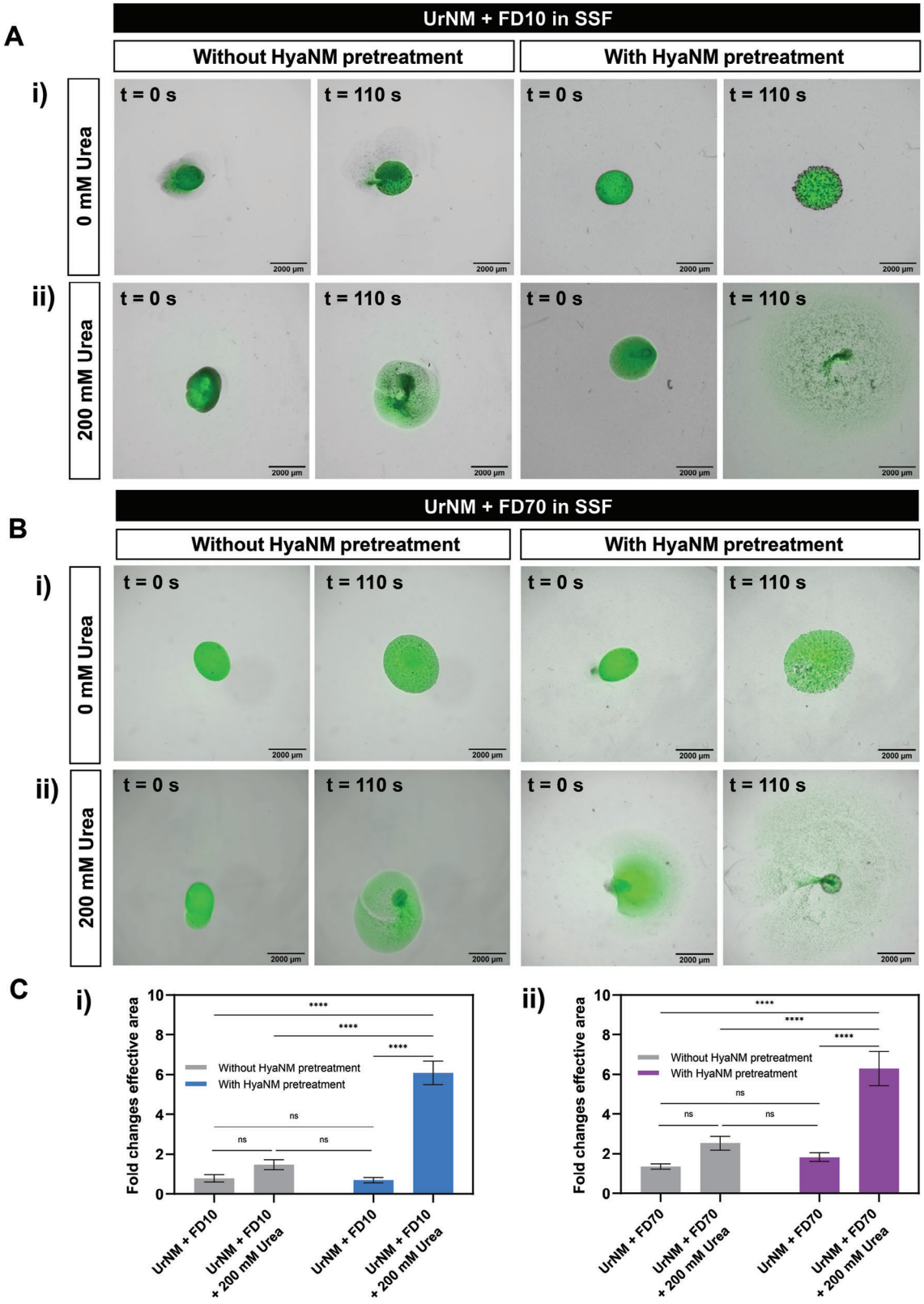

Figure 6. Analysis of FD diffusion when combined with UrNMs in SSF. Video screenshots in SSF of UrNMs and A) FD10 and B) FD70 without and with pretreatment with HyaNMs for 4 h and i) without and ii) with urea (200 mM). Scale bar = 2 mm. C) Fold changes in effective area covered by UrNMs and i) FD10 or ii) FD70, between times $t = 0$ and $t = 110$ s, for SSF with and without HyaNM treatment, and each of those with and without urea ($N = 9$, results are shown as mean ± SE). Asterisks denote a significant difference from the control with $^{****}p \leq 0.0001$.

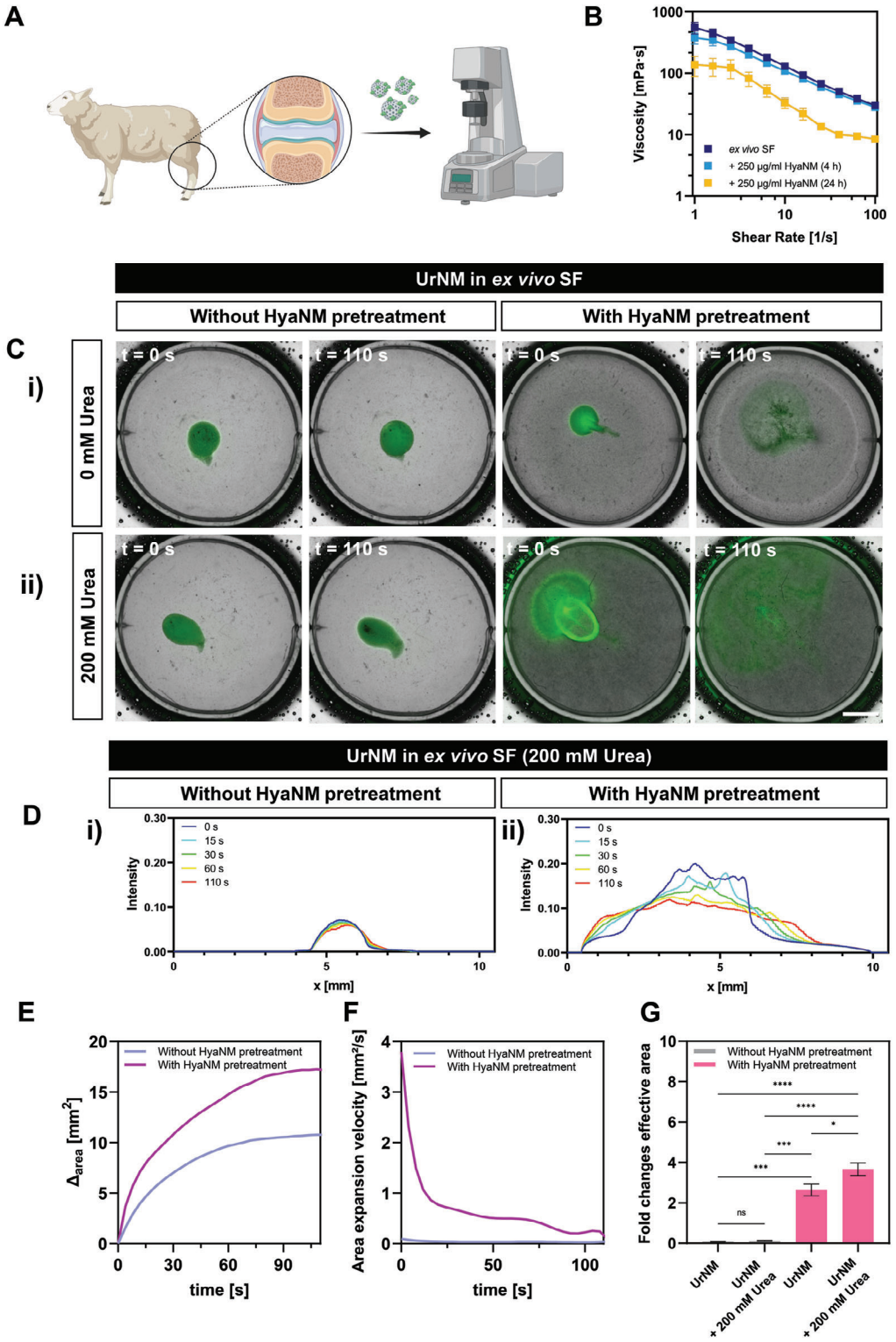

Figure 7. Analysis of UrNMs swarming behavior in ex vivo SF. A) Scheme illustrating ex vivo SF collection and rheological characterization. B) Viscosity versus shear rate of ex vivo SF with HyaNM pretreatment for different time durations. C) Video screenshots of UrNMs and FD70, without and with HyaNM treatment in ex vivo SF, i) without and ii) with urea (200 mM). Scale bar = 2 mm. D) Projections of the average pixel intensity along the *y*-axis for UrNMs in ex vivo SF with 200 mM of urea and i) without and ii) with HyaNMs pretreatment. E) Delta area covered by UrNMs and FD70 in ex vivo SF with 200 mM of urea with respect to time 0 s with and without HyaNM pretreatment. F) The area expansion velocity represents the growth in area covered per unit time and is the derivative of the plots panel E. G) Fold changes in effective area covered by UrNMs and FD70 between times $t = 0$ and $t = 110$ s, for ex vivo SF with and without HyaNM treatment, and each of those with and without urea ($N = 9$, results are shown as mean ± SE). Asterisks denote a significant difference from the control with: $^{*}p \leq 0.05$, $^{***}p \leq 0.001$, $^{****}p \leq 0.0001$.

in troops can enhance the diffusion of macromolecules such as FD70 in an ex vivo SF from sheep. Due to the high inter-sample variability, we homogenized them by batch mixing. We assessed the rheological changes in bulk viscosity of ex vivo SF in the presence of HyaNMs following the scheme shown in **Figure 7A**. The ex vivo SF (350 µL) containing HyaNMs (10 µL, 10 mg mL^{-1}) was placed in a rheometer, increasing the HyaNM concentration to 250 µg mL^{-1} as in the in vitro experiments. The ex vivo SF showed a classic shear thinning behavior (Figure 7B), as observed previously in the literature.[57] At a 1 s^{-1} shear rate, the viscosity of ex vivo SF was measured as 553.9 ± 119.5 mPa s, which the presence of HyaNMs had reduced to 376.4 ± 78.3 mPa s after 4 h. By continuing the HyaNM pretreatment for a total of 24 h we were able to decrease the SF viscosity by over 75% to 137.7 ± 50.0 mPa s, a necessary requirement to guarantee UrNMs movement. The reason why it took more time to achieve this reduction in viscosity is likely due to the more complex environment present in the medium's matrix, which is composed of HA, salts, proteins, and cells.

To study the diffusion of FD70 mediated by UrNMs motion, we placed a mixture containing UrNMs and FD70 into a homemade printed well, filled with ex vivo SF with and without HyaNMs and each of those with and without urea. UrNMs self-propulsion were analyzed in four different scenarios, with and without HyaNMs and each of those with and without urea (Figure 7C). The results were recorded on video for 110 s to visualize the temporal evolution of UrNMs and FD70 areal coverage (Movie S6, Supporting Information).

In the absence of urea, the UrNMs were unable to use self-propulsion and as a result the FD70 did not diffuse well, unless the ex vivo SF was pretreated with HyaNMs for 24 h (Figure 7C i) to reduce the viscosity. With urea (200 mM) and without HyaNM pretreatment, most UrNMs settled near the seed point, unable to swim in the highly viscous medium. In contrast, with 24 h of HyaNM pretreatment, the UrNMs with urea showed a pronounced diffusion, allowing FD70 to spread across almost all the entire Petri dish in 110 s (Figure 7C ii). The average pixel intensity along a line running through the center of the particle cloud clearly confirmed the above interpretations, showing the rapid expansion of the UrNMs particle cloud with HyaNM pretreatment (Figure 7D). The evolution of the effective area over time shows similar trends for FD70, i.e., the effective area increases monotonously until reaching an asymptotic limit after about 90 s (Figure 7E), with HyaNM pretreatment clearly leading to a significantly increased reach. The FD70 effective area after 110 s was 10.8 and 17.2 mm^2 without and with HyaNM pretreatment, respectively. Fitting a polynomial function to the effective area curves and calculating the time derivative we obtain the velocities of effective area expansion (Figure 7F). Without HyaNM pretreatment, this velocity started out at 0.095 mm^2 s^{-1} and decreased to 0.04 mm^2 s^{-1} at time 110 s, i.e., it remained close to zero throughout. In contrast, with HyaNM pretreatment, the effective area initially expanded rather rapidly at 3.79 mm^2 s^{-1} when the UrNMs first came into contact with urea. As the fuel was being used up, the velocity decreased continuously, mirroring the asymptotic part of the curve from Figure 7E, although never reaching the low values of the untreated scenario.

In terms of fold changes, without HyaNM pretreatment the area covered by FD70 and UrNMs without and with urea increased 0.9-fold (± 0.02) and 0.1-fold (± 0.02), respectively (Figure 7G). These differences were not statistically significant. If ex vivo SF was pretreated with HyaNMs, we observed statistically significant differences between the scenarios without and with urea, yielding area fold increases of 2.6 (± 0.3) and 3.8 (± 0.3), respectively.

In summary, we could demonstrate that FD were able to diffuse in ex vivo SF once its viscosity had been reduced by pretreating the SF with HyaNMs. Adding a second type of NM, UrNMs, led to a further increase in diffusion as long as urea was present to fuel self-propulsion. This successful proof of concept has great potential to pave the way for future sophisticated joint therapies.

4. Conclusion

In conclusion, we have successfully modified mesoporous silica nanoparticles with two different enzymes, namely hyaluronidase and urease, creating two troops of nanomotors whose combined actuation led to a reduction of SF viscosity and increased active diffusion of macromolecules, both in a simulated environment and ex vivo. Adding just UrNMs to SF resulted in no motion. We demonstrate that this issue can be overcome by pretreating the medium with HyaNMs to decrease the viscosity of the fluid. Hence, UrNMs show movement at single and collective scenarios. Moreover, HyaNMs catalytic activity can be depleted by the pH increase resulting from the UrNMs performance. Then, the combined effect of these two NMs troops was the increased diffusion of macromolecules, allowing them to spread to larger areas. The same results were obtained in simulated SF and ex vivo SF media.

Overall, we demonstrated that combining troops of NMs is useful in viscous media as the synergistic effect between ECM modification and fluid mixing leads to a considerable improvement in macromolecule diffusion. This will have wide-ranging implications for NMs applications in biomedicine, allowing researchers to transcend some of the limitations encountered in current therapeutic treatment approaches.

Supporting Information

Supporting Information is available from the Wiley Online Library or from the author.

Acknowledgements

This research was funded by the European Research Council (ERC) under the European Union's Horizon 2020 research and innovation program (grant agreement no. 866348; i-NanoSwarms), the Spanish Ministry of Science (grants PID2021-128417OB-I00 and RETI2018-098164-B-I00 funded by MCIN/AEI/10.13039/501100011033), by "ERDF A way of making Europe," and by Fundación Garcia Cugat. N.R.G. gratefully acknowledges the Spanish Ministry of Science for funding her predoctoral fellowship (PRE2019-088801). J.C.F gratefully acknowledges the Beatriu de Pinós Programme (2021-BP-00079). The authors thank Shuqin Chen for the mold design to perform side-view swarm study. The authors extend their gratitude for the assistance provided by Fundación García Cugat. Some of the figures were created with BioRender.com. Editorial assistance, in the form of language editing and correction, was provided by XpertScientific Editing and Consulting Services.

Conflict of Interest

The authors declare no conflict of interest.

Author Contributions

N.R.G. and M.G.C. synthesized the nanomotors and performed their characterization. N.R.G. performed the motion experiments, image processing, and data analysis. J.C.F. helped set up the fluorescence macromolecule model for the video recordings. N.R.G. and D.E.U conceptually designed and performed the rheological and electronic microscopy characterization and data analysis. A.C.B. contributed to the computational analysis. R.C., J.M.C., M.G.B., and P.L. provided valuable medical background information regarding the clinical need for NM applications. J.M.C. provided the ex vivo synovial fluid from sheep. N.R.G. and D.E.U. wrote the first draft of the manuscript. N.R.G., D.E.U., A.C.H., J.C.F., A.C.B, M.G.C., T.P., and S.S. revised the manuscript. S.S. and T.P. conceived the idea and project. S.S. supervised and administered the work. All authors have seen and approved this final version of the manuscript.

Data Availability Statement

The data that support the findings of this study are available on request from the corresponding author. The data are not publicly available due to privacy or ethical restrictions.

Keywords

collective motion, nanomotors, nanorobots, swarming, viscous media

Received: October 17, 2023
Published online: January 10, 2024

[1] M. J. Mitchell, M. M. Billingsley, R. M. Haley, M. E. Wechsler, N. A. Peppas, R. Langer, *Nat. Rev. Drug Discovery* **2021**, *20*, 101.
[2] S. Zhang, H. Uludag, *Pharm. Res.* **2009**, *26*, 1561.
[3] W. Poon, B. R. Kingston, B. Ouyang, W. Ngo, W. C. W. Chan, *Nat. Nanotechnol.* **2020**, *15*, 819.
[4] E. Blanco, H. Shen, M. Ferrari, *Nat. Biotechnol.* **2015**, *33*, 941.
[5] B. Kichatov, A. Korshunov, V. Sudakov, V. Gubernov, A. Golubkov, A. Kiverin, A. Nastulyavichus, S. Kudryashov, *Phys. Chem. Chem. Phys.* **2023**, *25*, 11780.
[6] D. Schamel, A. G. Mark, J. G. Gibbs, C. Miksch, K. I. Morozov, A. M. Leshansky, P. Fischer, *ACS Nano* **2014**, *8*, 8794.
[7] Z. Wu, J. Troll, H.-H. Jeong, Q. Wei, M. Stang, F. Ziemssen, Z. Wang, M. Dong, S. Schnichels, T. Qiu, P. Fischer, *Sci. Adv.* **2018**, *4*, eaat4388.
[8] F. Striggow, M. Medina-Sánchez, G. K. Auernhammer, V. Magdanz, B. M. Friedrich, O. G. Schmidt, *Small* **2020**, *16*, 2000213.
[9] P. L. Venugopalan, A. Ghosh, *Langmuir* **2021**, *37*, 289.
[10] A. Aghakhani, A. Pena-Francesch, U. Bozuyuk, H. Cetin, P. Wrede, M. Sitti, *Sci. Adv.* **2022**, *8*, eabm5126.
[11] W. Chen, R. Jiang, X. Sun, S. Chen, X. Liu, M. Fu, X. Yan, X. Ma, *Chem. Mater.* **2022**, *34*, 7543.
[12] J. Meng, K. Wei, S. Xie, Z. Zhang, P. Ran, P. Zhang, X. Li, *J. Controlled Release* **2023**, *357*, 342.
[13] F. Zhang, J. Zhuang, Z. Li, H. Gong, B. E.-F. De Ávila, Y. Duan, Q. Zhang, J. Zhou, L. Yin, E. Karshalev, W. Gao, V. Nizet, R. H. Fang, L. Zhang, J. Wang, *Nat. Mater.* **2022**, *21*, 1324.
[14] B. E.-F. De Ávila, P. Angsantikul, J. Li, M. Angel Lopez-Ramirez, D. E. Ramírez-Herrera, S. Thamphiwatana, C. Chen, J. Delezuk, R. Samakapiruk, V. Ramez, M. Obonyo, L. Zhang, J. Wang, *Nat. Commun.* **2017**, *8*, 272.
[15] C. Xu, S. Wang, H. Wang, K. Liu, S. Zhang, B. Chen, H. Liu, F. Tong, F. Peng, Y. Tu, Y. Li, *Nano Lett.* **2021**, *21*, 1982.
[16] M. Mathesh, J. Sun, D. A. Wilson, *J. Mater. Chem. B* **2020**, *8*, 7319.
[17] X. Arqué, T. Patiño, S. Sánchez, *Chem. Sci.* **2022**, *13*, 9128.
[18] C. Xu, Y. Jiang, H. Wang, Y. Zhang, Y. Ye, H. Qin, J. Gao, Q. Dan, L. Du, L. Liu, F. Peng, Y. Li, Y. Tu, *Adv. Sci.* **2023**, *10*, 2204881.
[19] D. Walker, B. T. Käsdorf, H.-H. Jeong, O. Lieleg, P. Fischer, *Sci. Adv.* **2015**, *1*, 1500501.
[20] H. Choi, S. H. Jeong, T. Y. Kim, J. Yi, S. K. Hahn, *Bioact Mater* **2022**, *9*, 54.
[21] M. A. Ramos-Docampo, M. Fernández-Medina, E. Taipaleenmäki, O. Hovorka, V. Salgueiriño, B. Städler, *ACS Nano* **2019**, *13*, 12192.
[22] M. A. Ramos Docampo, N. Wang, S. Pendlmayr, B. Städler, *ACS Appl. Nano Mater* **2022**, *5*, 14622.
[23] F. Rajabasadi, S. Moreno, K. Fichna, A. Aziz, D. Appelhans, O. G. Schmidt, M. Medina-Sánchez, *Adv. Mater.* **2022**, *34*, 2204257.
[24] Z. Zhang, D. Zhang, B. Qiu, W. Cao, Y. Liu, Q. Liu, X. Li, *Nanoscale* **2021**, *13*, 6545.
[25] A. C. Hortelao, C. Simó, M. Guix, S. Guallar-Garrido, E. Julián, D. Vilela, L. Rejc, P. Ramos-Cabrer, U. Cossío, V. Gómez-Vallejo, T. Patiño, J. Llop, S. Sánchez, *Sci Robot* **2021**, *6*, eabd2823.
[26] J. C. Fraire, M. Guix, A. C. Hortelao, N. Ruiz-González, A. C. Bakenecker, P. Ramezani, C. Hinnekens, F. Sauvage, S. C. De Smedt, K. Braeckmans, S. Sánchez, *ACS Nano* **2023**, *17*, 7180.
[27] W. Stöber, A. Fink, E. Bohn, *J. Colloid. Interface Sci.* **1968**, *26*, 62.
[28] A. Simon, V. R. De Almeida Borges, L. M. Cabral, V. P. De Sousa, *AAPS PharmSciTech* **2013**, *14*, 425.
[29] S. D. Conzone, R. F. Brown, D. E. Day, G. J. Ehrhardt, *J Biomed. Mater. Res.* **2002**, *60*, 260.
[30] M. R. C. Marques, R. Loebenberg, M. Almukainzi, *Dissolution Technol.* **2011**, *18*, 15.
[31] T. Patiño, N. Feiner-Gracia, X. Arqué, A. Miguel-López, A. Jannasch, T. Stumpp, E. Schäffer, L. Albertazzi, S. Sánchez, *J. Am. Chem. Soc.* **2018**, *140*, 7896.
[32] T. Patiño, X. Arqué, R. Mestre, L. Palacios, S. Sánchez, *Acc. Chem. Res.* **2018**, *51*, 2662.
[33] C. Xiang, F. Yang, M. Li, M. Jaridi, N. Wu, *J. Nanoparticle Res.* **2013**, *15*, 1293.
[34] Z. G. Peng, K. Hidajat, M. S. Uddin, *J. Colloid Interface Sci.* **2004**, *271*, 277.
[35] P. Schaufuss, R. Sting, W. Schaeg, H. Blobel, *Zent.bl. Bakteriol.* **1989**, *271*, 46.
[36] S. Palagi, D. Walker, T. Qiu, P. Fischer, in *Microbiorobotics*, Elsevier, Amsterdam **2017**, pp. 133–162.
[37] P. Tekiner, I. Perçin, B. Ergün, H. Yavuz, E. Aksöz, *J. Mol. Recognit.* **2012**, *25*, 549.
[38] J. P. Celli, B. S. Turner, N. H. Afdhal, S. Keates, I. Ghiran, C. P. Kelly, R. H. Ewoldt, G. H. Mckinley, P. So, S. Erramilli, R. Bansil, *Proc Natl Acad Sci U S A* **2009**, *106*, 14321.
[39] X. Cao, R. Bansil, K. R. Bhaskar, B. S. Turner, J. T. Lamont, N. Niu, N. H. Afdhal, *Biophys. J.* **1999**, *76*, 1250.
[40] J. P. Celli, B. S. Turner, N. H. Afdhal, R. H. Ewoldt, G. H. Mckinley, R. Bansil, S. Erramilli, *Biomacromolecules* **2007**, *8*, 1580.
[41] T. M. Tamer, *Interdiscip Toxicol* **2013**, *6*, 111.
[42] G. W. Greene, X. Banquy, D. W. Lee, D. D. Lowrey, J. Yu, J. N. Israelachvili, *Proc Natl Acad Sci U S A* **2011**, *108*, 5255.
[43] E. Bortel, B. Charbonnier, R. Heuberger, *Lubricants* **2015**, *3*, 664.
[44] A. Fallacara, E. Baldini, S. Manfredini, S. Vertuani, *Polymers* **2018**, *10*, 701.
[45] Z. Zhang, G. F. Christopher, *Soft Matter* **2015**, *11*, 2596.

[46] A. Maleki, A.-L. Kjøniksen, B. Nyström, *Macromol. Symp.* **2008**, *274*, 131.
[47] A. Dodero, R. Williams, S. Gagliardi, S. Vicini, M. Alloisio, M. Castellano, *Carbohydr. Polym.* **2019**, *203*, 349.
[48] R. H. Colby, *Rheol. Acta* **2010**, *49*, 425.
[49] M. Unni, S. Savliwala, B. D. Partain, L. Maldonado-Camargo, Q. Zhang, S. Narayanan, E. M. Dufresne, J. Ilavsky, P. Grybos, A. Koziol, P. Maj, R. Szczygiel, K. D. Allen, C. M. Rinaldi-Ramos, *Sci. Adv.* **2021**, *7*, eabf8467.
[50] E. Kutálková, J. Hrnčiřík, R. Witasek, M. Ingr, *Carbohydr. Polym.* **2020**, *234*, 115919.
[51] M. K. Cowman, T. A. Schmidt, P. Raghavan, A. Stecco, *F1000Res.* **2015**, *4*, 622.
[52] S. P. Zhong, D. Campoccia, P. J. Doherty, R. L. Williams, L. Benedetti, D. F. Williams, *Biomaterials* **1994**, *15*, 359.
[53] P. J. Hotez, S. Narasimhan, J. Haggerty, L. Milstone, V. Bhopale, G. A. Schad, F. F. Richards, *Infect. Immun.* **1992**, *60*, 1018.
[54] R. Golestanian, T. B. Liverpool, A. Ajdari, *Phys. Rev. Lett.* **2005**, *94*, 220801.
[55] J. R. Howse, R. A. L. Jones, A. J. Ryan, T. Gough, R. Vafabakhsh, R. Golestanian, *Phys. Rev. Lett.* **2007**, *99*, 048102.
[56] M. Sánchez, E. Anitua, G. Orive, I. Mujika, I. Andia, *Sport. Med.* **2009**, *39*, 345.
[57] A. Ö. Bingöl, D. Lohmann, K. Püschel, W.-M. Kulicke, *Biorheology* **2010**, *47*, 205.

